Journal of Colloid and Interface Science 538 (2019) 209–217

Contents lists available at ScienceDirect

Journal of Colloid and Interface Science

journal homepage: www.elsevier.com/locate/jcis

Sandwich layering in binary nanoparticle films and effect of size ratio on stratification behavior

Weiping Liu [a], Amanda J. Carr [a], Kevin G. Yager [b], Alexander F. Routh [c], Surita R. Bhatia [a,*]

[a] Department of Chemistry, Stony Brook University, Stony Brook, NY, USA
[b] Center for Functionalized Nanomaterials, Brookhaven National Laboratory, Upton, NY, USA
[c] Department of Chemical Engineering and Biotechnology, University of Cambridge, Pembroke Street, Cambridge CB2 3RA, United Kingdom

GRAPHICAL ABSTRACT

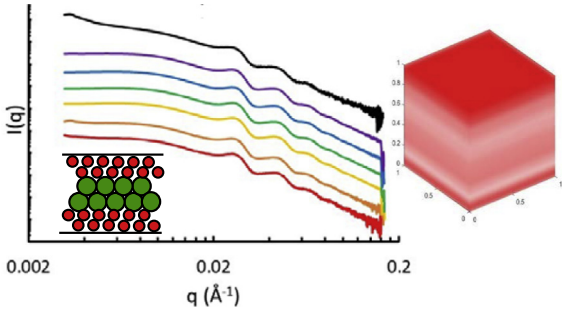

ARTICLE INFO

Article history:
Received 14 September 2018
Revised 21 November 2018
Accepted 22 November 2018
Available online 23 November 2018

Keywords:
Film formation
Evaporative assembly
Drying
Stratification
Colloidal films

ABSTRACT

Hypothesis: Stratification or self-segregation of multicomponent particle mixtures during drying is an important phenomenon to understand for the development of single-step deposition processes for complex coatings. We hypothesize that varying the ratio of particle Peclet numbers will lead to different types of stratification behavior.

Experiments: Binary colloidal films of polystyrene and silica were prepared by evaporative film formation, and stratification of nanoparticles of different size ratio (7.7–1.2) was studied using microbeam small-angle X-ray scattering (SAXS).

Findings: SAXS spectra showed noticeable variations at different film depths, consistent with stratification. These results are quantified to obtain vertical composition profiles. We observe "sandwich"-type layered structures at different nanoparticle size ratios, which to our knowledge have not been previously observed experimentally or predicted by theory. For example, for films of larger particle size ratios (7.7–4.8), large particles are enriched at the film top and bottom, leading to a large-small-large or "LSL" behavior; while within films of smaller particle size ratio (2.2–1.2), small particles are enriched at the top and bottom of the film (small-large-small or "SLS" structures). The enrichment of particles at the top persists over several hundred particle layers and is not just a single monolayer pinned to the upper surface.

1. Introduction

Multicomponent films prepared from drying colloidal and nanoparticle suspensions have a wide range of applications. Multifunctional coatings are in demand for various purposes; for

* Corresponding author.
E-mail address: surita.bhatia@stonybrook.edu (S.R. Bhatia).

https://doi.org/10.1016/j.jcis.2018.11.084
0021-9797/

example, corrosion-resistant coatings for metal substrates and antibacterial coatings for home furnishings, where only the surface of the film requires special functionality. Other advanced applications of multicomponent films include 3D printing [1], batteries for energy storage [2,3], anti-reflective coatings [4], electronic devices [5,6], and medical diagnostic tools [7]. Traditionally, multicomponent coatings with vertical structures are achieved by a multi-step deposition technique, which can be costly and time-consuming. Therefore, it is desirable to develop a single-step method where a multifunctional film can be prepared by casting and drying colloidal suspensions on substrates [8].

The film formation process can be characterized by four stages, with three transformations between them [9–11]. The first transformation occurs as solvent evaporates and particles become close-packed [12]. This is followed by particle deformation, where forces arising from dry sintering, capillary effects, or wet sintering cause close-packed spherical particles to deform into a space-filling polyhedrons [12–14]. Finally, interdiffusion between particles forms a continuous film [13,14]. This work focuses on the first stage of drying, where particles distribute themselves during solvent evaporation. It is in this stage where vertical stratification may occur.

During the drying process, Routh and Russel [12–14] showed that particle distributions are affected by the Peclet number, which is defined as the rate of evaporation divided by the rate of diffusion and given as

$$Pe = \frac{6\pi\eta RHE}{kT} \tag{1}$$

where η is the solvent viscosity, R is the particle radius, H is the initial film thickness, E is the rate of evaporation, k is Boltzmann's constant, and T is the temperature. When $Pe << 1$, diffusion is fast enough that particles distribute themselves evenly throughout the film; when $Pe >> 1$, evaporation dominates, and particles will be trapped at the upper surface as drying occurs. This definition of Pe is based on the Einstein-Stokes relation for particle diffusion, which strictly only applies in the early stages of drying when dispersions are dilute. As drying proceeds and dispersions becomes more concentrated, particle motion will slow down, even to the point where particles may become jammed. We do not claim that this is an appropriate description of particle motion throughout the drying process; however, as this definition of Pe has been widely used in modeling film formation [12–14] and describing stratification behavior [15–19], we will use it here to aid in comparing our results to previous work.

Trueman et al. [15] first predicted that, when a binary colloidal system has two types of particles with Pe straddling unity, i.e. $Pe_1 < 1$ and $Pe_2 > 1$ (in this work, we denote Pe_1 and Pe_2 as the Peclet numbers for small and large particles, respectively), particles may distribute themselves vertically during drying. In this case, large particles, which have a larger Pe, are predicted to be enriched at the air-film interface, while small particles will diffuse uniformly within the film, i.e. stratification occurs [15]. Experimental AFM studies using a binary system with polymeric particles have been performed to verify this model [16]. The experimental results were in general agreement with predicted trends, but only qualitatively. Additionally, as AFM studies are only able to probe the top surface of the films, these experiments did not provide insight into vertical concentration profiles within the films.

Other experimental studies have shown the importance of particle interactions to the stratification behavior. For example, Nikiforow et al. [8] studied systems with charged and neutral particles and found that neutral particles were preferentially enriched on the top of films. Routh and co-workers modified their diffusive model to incorporate the effects of particle interaction and determined that attractions between large particles as well as repulsion between small particles, regardless of the interaction between large and small particles, can facilitate the stratification along with hydrodynamic effects [17]. Cheng and Grest [18] performed large-scale molecular dynamics simulations on dispersions containing large polymeric particles and small nanoparticles, and they demonstrated that, if interactions between large particles and small nanoparticles are stronger than those between the solvent and small nanoparticles, this can result in a nanoparticle-enriched interface. However, if there are strong interactions between the solvent and small nanoparticles, this can result in large particles being enriched at the interface, under conditions of fast evaporation ($Pe >> 1$ for both particles).

Francis et al. [20] first reported stratification phenomenon in drying binary mixtures of polymeric and ceramic particles. However, they focused on systems prepared at relatively high temperature, i.e. under fast evaporation. In addition, relatively large particle sizes were used, resulting in Pe_1 of 120 and Pe_2 of 460. Therefore, it is likely that the stratification behavior they observe is due to a different mechanism than that proposed by the diffusive model of Trueman et al. Francis and co-workers created films with small particles enriched at the interface and large particles enriched within the body of the film, which can be described as inverted stratification. They proposed, as a possible mechanism for the inverted stratification, that the existence of some very small ceramic nanoparticles might be able to diffuse into the interstitial spaces among latex particles. This might also be attributed to the fact that the relative rate of diffusion of the two particles become less important when both particles have very high Peclet numbers ($Pe >> 1$), since in this case evaporation occurs much more rapidly than particle diffusion, even for small particles.

Many recent theoretical studies predict an inverted stratification structure, where small particles are enriched at the top surface and large particles were pushed to the bottom, though most of these systems used relatively fast evaporation rates, i.e. both particles have Peclet numbers >> 1. Fortini et al. [19] performed simulations of drying binary colloidal mixtures with Pe_1 of 75 and Pe_2 of 525. Complementary experiments were also performed with Pe_1 of 14 and Pe_2 of 100. Both simulations and experiments found that the air-film interface was enriched with small particles, and the body of film was enriched with large particles. They proposed that an osmotic pressure gradient would push large particles downward to the bottom of the film, which might be account for the inverted stratification. Later Fortini and Sear extended their conclusions to ternary mixtures and polydisperse colloidal systems [21]. Panagiotopoulos and co-workers [22] performed implicit-solvent molecular dynamic simulations with similar systems and conditions as Fortini et al. Inverted stratification was also observed in their results. They proposed that the difference in chemical potential gradients of particles outweighs the effects of the counteraction of friction coefficient on migration velocities of particles. Moreover, their results suggested that this inverted stratification not only occurs under fast evaporation but also moderate evaporation, i.e. $Pe_1 \approx 1$ and $Pe_2 >> 1$, although to a lesser extent. They found that large particle size ratios sped up and enhanced the establishment of the stratified layers. Additional work of Panagiotopoulos has focused on the stratification of drying polymer-polymer and colloid-polymer binary mixtures, and the results showed good agreement with their previous work on binary colloidal mixtures [23]. Zhou et al. [24] also predicted inverted stratification in binary mixtures. Their simulation results rely on an asymmetric cross interaction between large and small particles to obtain this result. Interestingly, they found that the condition for this inverted stratification to occur only depends on the particle size ratio, Pe for the small particles, and the volume fraction of small particles. The condition for inverted stratification to occur is given as,

$$\alpha^2(1+Pe_1)\Phi_{01} > 1 \quad (2)$$

where α is the size ratio between large and small particle and Φ_{01} is the initial volume fraction for small particles. Recently, Sear and Warren [25] used the Asakura-Oosawa polymer model to suggest a mechanism of the inverted stratification. Their model took the effect of solvent backflow into account and should not significantly overestimate the effects of diffusiophoretic drift, a concern with some earlier studies [19,21–24]. Finally, very recent studies of Sear [26] and by Cheng and co-workers [27] include an explicit solvent in molecular dynamics simulations. Their results show both small-on-top and large-on-top regimes of stratification but suggest that the implicit solvent approach used by Zhou et al. overestimates small-on-top aggregation. Their results, together with the work of Sear and Warren [25], lead to a condition for small-on-top stratification of $Pe_s\phi_s \gtrsim C$, where C is found to be 0.64 by Sear [26], ~2 by Sear and Warren [25], and ~1 by Cheng and co-workers [27].

Concurrent with these advanced theory and simulations, recent experimental studies have demonstrated different types of stratification behavior. Previous experimental studies in our group [28] utilizing AFM have shown that both the particle size ratio and processing factors are important for the distribution of particles in drying colloidal mixtures. Humidity, for example, can affect the evaporation rate, and thus the Peclet numbers. In one case, good humidity control allowed particles to have Peclet numbers straddling unity and to have the largest number of large particles migrate to the top surface, which was in general agreement with Routh's predictions. Results also suggested that, while Pe_1 and Pe_2 were set to straddle unity, a larger particle size ratio would decrease the extent of stratification; i.e., result in more small particles on top. We proposed that large particle size ratios might induce depletion attractions, causing aggregation of large particles which then migrate to the bottom of the film. Similar mechanisms have been discussed by others [16,20]. However, AFM characterization only probes the surface of the film over a small area, making it difficult to draw quantitative conclusions. Similarly, Makepeace et al. [29] recently used AFM to perform surface characterization and study the effects of particle size ratio and concentration of small particles on stratification. They found qualitative agreement in experiments and simulations with the theory proposed by Zhou et al. [24] Cryo-SEM was applied to obtain cross-sectional images as well. Nevertheless, their experiments presented the same limitation as our previous AFM studies, and their implicit-solvent simulations still overestimated the degree of stratification.

In this work, we prepared nanoparticle films with polystyrene and silica particles of different sizes and studied how stratification was affected by different nanoparticle size ratios. As discussed below, our results show behavior beyond the "small-on-top" and "large-on-top" structures predicted by theory, yielding small-large-small and large-small-large layering behavior. While computational and experimental results from Francis et al. showed that, for one-component dispersions, particles can migrate to either interface and be present in relatively small amounts at the center of the film if the evaporation rate, sedimentation rate, and diffusion are well-controlled [30], "sandwich" structures in binary systems, where one type of particle enriches the top and bottom of the film, and another is enriched the center of films, have not been seen or predicted before. Probing the depth-resolved particle composition is enabled through the use of a novel microbeam small-angle X-ray scattering (SAXS) approach that we have described in a previous paper [31], which can give more quantitative results of the particle volume fractions throughout the film thickness. These experiments involve conducting a vertical scan throughout the film and require a narrowly-focused beam with high intensity. Furthermore, SAXS is an attractive approach for studying drying of colloidal mixtures, since it provides good vertical resolution with corresponding quantification of nanoscale packing, and is relatively non-destructive. Although beam damage may occur with polymeric samples if they are exposed to synchrotron radiation for long times, in our experiments we find that modest acquisition times at any given vertical position in the film do not generate beam damage in dried colloidal films. Dingenouts and Ballauff used SAXS techniques to explore structure changes of latex films upon drying and their results indicated a liquid-like short range order instead of crystallinity within the dried films [32,33] Goehring et al. performed dip-coating to make colloidal films and conducted SAXS experiments to follow variation of scattering patterns at different times. Similarly, they found the lack of long range order in the final films, while short range order presented for a small period at the liquid-solid transition. Additionally, their results could follow volume fraction variations and capture structure changes in transitions between stages during drying. The results also indicated no significant far-field flow was present to affect distribution of the number of particles at different positions horizontally [34]. We believe our work can be used to guide future work on modelling the dynamics of multicomponent film formation by evaporative assembly, and can be inspiring for industrial applications to better design systems for making multifunctional films with desired compositions.

2. Experiments

2.1. Materials

In the experiments, polystyrene (PS) particles in aqueous suspensions were obtained from Invitrogen, and silica nanoparticles (Ludox) were obtained from Sigma-Aldrich and Grace (lot numbers are provided in Supplemental Information). Sample details and measured particle diameters and zeta potential are listed in Table 1. The particle radii were determined by performing three to four 5-min measurements, at 25 °C, pH = 9 (approximate to silica suspension storage pH value) with a NanoBrook Omni dynamic light scattering instrument (Brookhaven Instruments), which has a wavelength of 640 nm. In the resulting size distributions, minor scattering peaks potentially from aggregates, precursors and dust were omitted to obtain accurate particle sizes. Zeta potential measurements were conducted with three to four repeats using the NanoBrook Omni instrument. Sample names refer to the material type and the nominal radii in nm. With the measured particle sizes and material densities reported in the literature (2.65 g/cm^3 for silica and 1.04 g/cm^3 for polystyrene) [35,36], the Stokes settling velocity of particles U_0 can be calculated as,

$$U_0 = \frac{2R^2\Delta\rho g}{9\mu} \quad (3)$$

where R is the radii of particle, $\Delta\rho$ is the difference between the density of particle and of solvent, g is the gravitational constant and μ is the solvent viscosity. For all the particles used in this paper, the U_0 are small ($\leq 1.63 \times 10^{-9}$ m/s) and can be neglected on the time scales of the drying process. If large aggregates formed during the drying process, we would expect these to have a faster sedimentation rate, which might affect the final particle However, the absence of aggregation was confirmed in SAXS spectra, as no dramatic increase of intensity at low q was observed, which would be expected if there were any large aggregates formed.

2.2. Sample preparation

To prepare colloidal films, polystyrene and silica suspensions were first diluted to 3% v/v with a solution of NaOH in distilled water at pH = 9. To make pure polystyrene or pure silica films,

Table 1
Sample names, measured particle radii and zeta potential, and calculated Pecelt numbers. Uncertainties in radii and zeta potential are based on the standard deviation from 3 to 4 measurements, and uncertainty in *Pe* is based on relative uncertainty in measured radii.

Content	Name	Radius (nm)	Peclet Number	Zeta Potential (mV)
Polystyrene	PS-48	47.9 ± 0.0	10.4 ± 0.0	−48.9 ± 4.3
Polystyrene	PS-21	21.4 ± 1.2	4.6 ± 0.3	−68.0 ± 3.4
Silica	Silica-17	17.2 ± 1.8	3.7 ± 0.4	57.4 ± 2.9
Silica	Silica-10	9.9 ± 0.5	2.1 ± 0.1	57.0 ± 4.5
Silica	Silica-8	8.4 ± 1.1	1.8 ± 0.2	73.2 ± 2.1
Silica	Silica-6	6.2 ± 0.2	1.3 ± 0.1	57.2 ± 4.5

the diluted suspensions were cast and dried; to make binary mixture films, equal volumes of diluted polystyrene and silica were mixed, and suspensions of 1.5% v/v of polystyrene and 1.5% v/v of silica were cast and dried. Each suspension was dried on a deep-well projection slide from Diatec AS, which has a diameter of 23.5 mm and a depth of 1.5 mm. The suspensions were then placed into an environmental chamber (Caron 6010) for the entire drying process, where the temperature was set at 40 °C, which is below the glass transition temperature of PS, and the humidity was set at 60%. The films were dried overnight. An illustration of the projection slides, pictures of dried films and a similar experimental process was available in a previous paper [28].

The Peclet numbers can be calculated for this drying condition, using a solvent viscosity of 6.5143×10^{-4} Pa s and density of 0.9922 g/cm^{-3} at 40 °C, an initial film thickness was 1.5 mm, and a rate of evaporation of 0.0786 g/h. The rate of evaporation was determined by averaging three measurements of the rate of evaporation of pure water in the same slide wells, and can be converted into the rate that the solvent front moves downward, which was 5.0734×10^{-8} m/s. The Peclet numbers for the particles are listed in Table 1.

2.3. Small angle X-ray scattering (SAXS)

SAXS experiments were performed at the Complex Materials Scattering (CMS, 11-BM) beamline at the National Synchrotron Light Source II (NSLS-II), Brookhaven National Laboratory (BNL). In the experiment, an X-ray micro-beam with a full-width half-maximum (vertical direction) of 26.6 μm was generated using a two-slit system. Sections of the films approximately 1–3 mm in the beam direction were placed on a stage and measured under vacuum to reduce background. No corrections were performed for sample adsorption due to the small sample dimension in the beam direction. Scattering intensity data were collected on a Dectris Pilatus 2M detector, covering a wave vector range of 0.003–5 Å^{-1}. During each scan X-ray beam passed through 26.6 μm thickness of the films, and films were then vertically moved by 10 μm for the next scan, where enhanced intensity were allowed by oversampling. SAXS data were acquired across the film at vertical spacings of 10 μm to extract volume fractions at each height of the film. Scattering intensity of each height was collected for films made with pure polystyrene, pure silica and the binary mixtures. Each scan took 30 s or 120 s to achieve good resolution.

For each vertical scan, some images at the very beginning or end of the scan exhibit low signal, as the X-ray beam is not fully intersecting the sample; these data were excluded from analysis. Scattering intensity was normalized by acquisition time. Background subtraction was not required due to the in-vacuum measurements (which eliminates scattering from windows and air) and the low detector background. In the plots presented below, film depths are scaled and normalized on the total film thickness, so that the scaled depth ranges from 0 to 1, where 1 represents the top of the film (vacuum interface) and 0 represents the bottom (substrate interface).

The two-dimensional flatfield-corrected detector image was converted into a one-dimensional I vs. q curve by circular averaging (i.e. computing the average scattering intensity for every total q value). Masked detector regions are excluded from the circular average intensity (photon counts per pixel) calculation. The mask used for the analysis herein accounted for the intermodule gaps that appear in the Pilatus 2M detector, as well as the linear beamstop used to block the direct beam and any strong specular scattering arising as the beam crosses interfaces. Note that the masked circular average gives a robust $I(q)$ curve for nominally isotropic scattering signals. For anisotropic scattering, any kind of mask will introduce slight artifacts since one is excluding certain regions of q/angle space and not others, thereby biasing the average. The X-ray scattering signal for the studies herein was nominally isotropic when measuring the film interior, but became slightly anisotropic as one approaches either the substrate interface or the film top surface (owing to interface scattering and shadowing effects). This leads to small intensity artifacts in the $I(q)$ curves near these locations.

3. Results and discussion

3.1. Microbeam small-angle X-ray scattering

By performing SAXS on mixed PS/silica films, we obtained scattering patterns at different depths. In Fig. 1, data from representative depths are plotted. Fig. 1 also lists the total film thickness for each sample. Scattered intensity is plotted in arbitrary units; in the main plots, intensity has been shifted vertically to avoid overlap; in the insets, intensities are again shifted vertically to highlight any observed differences in peak intensity and position at different depths in the films.

Based on the sizes of silica and PS particles and scattering from pure silica and PS films (Supplementary Information), peaks corresponding to silica and PS in the mixed films were identified. Scattered intensities for different films in the q ranges assigned for primary peaks of silica particles are compared in the insets of Fig. 1, since silica scatters X-rays more strongly than polystyrene. Variations at different depths are clearly seen. In Fig. 1A and B, obvious differences of silica scattering peaks can be seen for large Peclet number ratios, i.e. nanoparticle size ratios of 7.7 and 5.7. Silica peak heights decreased along the normalized film depth 0.0–1.0. In Fig. 1C and D, for intermediate Peclet number ratios 4.8 and 2.8, the silica peak heights first increased from the bottoms towards the centers, and then decreased from the centers of the films towards the top surfaces. In Fig. 1E and F, most peaks remain unchanged at different depths for small Peclet number ratios 2.2 and 1.2, while the peak height at depth 1.0 in Fig. 1F appeared smaller than the others.

The comparisons of silica scattering peaks show evidence for stratification within the mixture films. Typically, stronger scattering peaks for silica indicate a larger volume fraction of silica particles in particular regions of the film. For comparison, insets of the regions corresponding to PS particles are provided in the Supple-

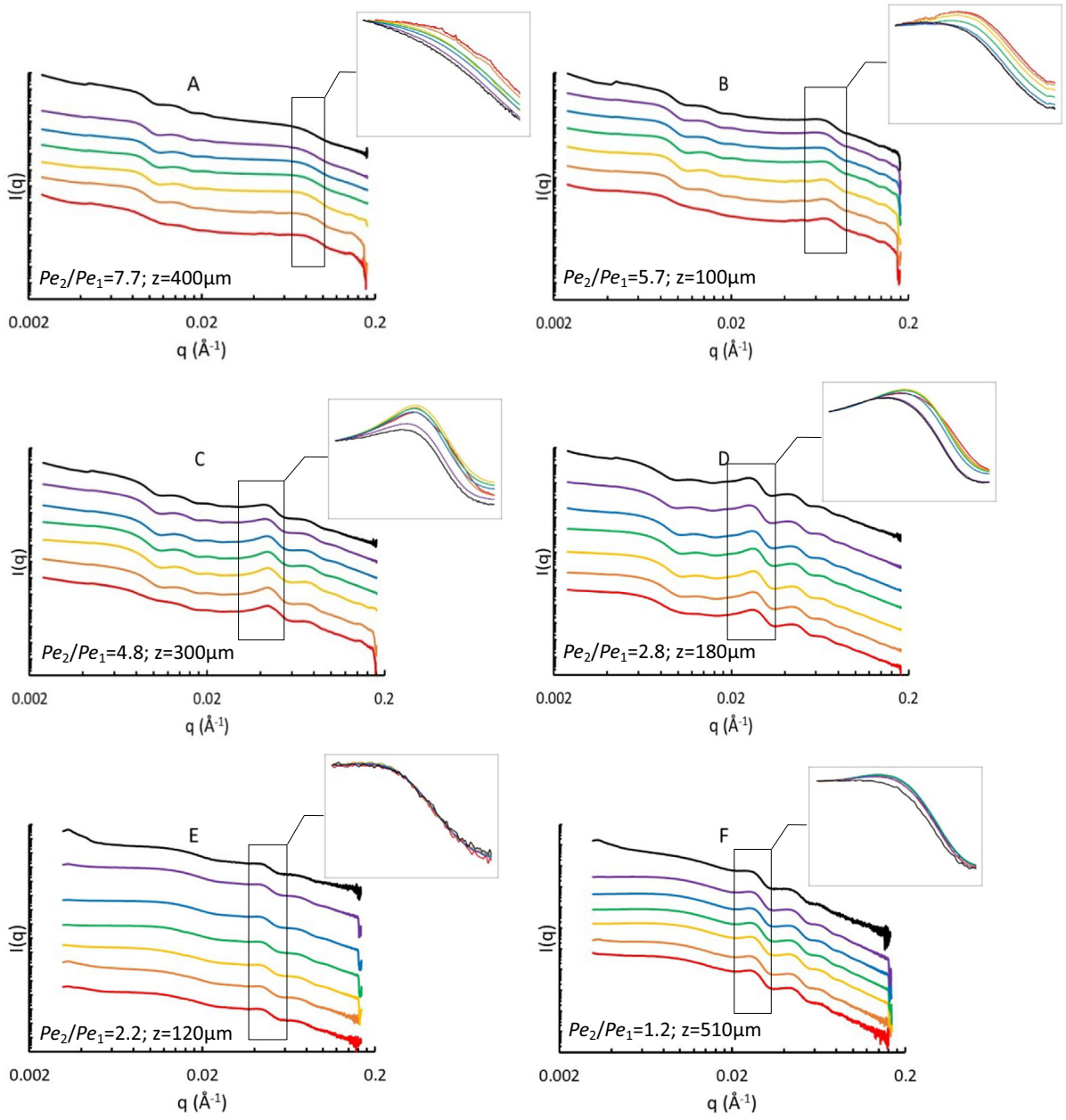

Fig. 1. Small-angle X-ray scattering at selected vertical positions of mixture films made with (A) PS-48 and Silica-6 (Pe_2/Pe_1 = 7.7); (B) PS-48 and Silica-8 (Pe_2/Pe_1 = 5.7); (C) PS-48 and Silica-10 (Pe_2/Pe_1 = 4.8); (D) PS-48 and Silica-17 (Pe_2/Pe_1 = 2.8); (E) PS-21 and Silica-10 (Pe_2/Pe_1 = 2.2); and (F) PS-21 and Silica-17 (Pe_2/Pe_1 = 1.2). Intensity and scattering vector are plotted in log-log scales for both main and inset graphs. Intensities are in arbitrary units and curves are shifted for clarity. From bottom to top, curves represent selected scaled film depths from 0.0 to 1.0. Comparisons of peak shapes at q ranges assigned as silica primary peaks are given.

mentary Information (Fig. S1), but trends are not as clear in these data, due to weaker scattering from the PS particles, compared to the silica particles.

3.2. Characterization of stratification behavior

In order to quantify the concentration profile throughout the film, we applied a linear combination analysis to the data, assuming the scattered intensity of the binary mixtures is equal to a weighted summation of scattering from dried films of pure polystyrene and silica. Note that this approach does not neglect interparticle interactions, as we base our fits on scattering from dried films of pure PS and pure silica particles, which are presumably at a concentration equivalent to random close packing, $\phi = 0.64$ and have broad peaks arising from interparticle interactions, characteristic of concentrated colloidal materials without long-range order. However, this approach does neglect any changes in the structure factor arising from the presence of a second particle type. For example, packing of two different sized particles could result in local configurations, and thus scattering signatures, not present in either pure system. However, our systems are disordered and do not show any signatures of long-range order, and so for the disordered colloidal materials studied here, a linear combination of the pure material scattering curves provides a reasonable approximation to the total scattering curve. Details of the fitting approach are given in supplemental information.

The silica volume fraction at different scaled film depths for binary mixture films are plotted in Fig. 2. The results of our data analysis are consistent with the qualitative discussion of the data in Fig. 1 in most cases; that is, in general our data fitting yields high

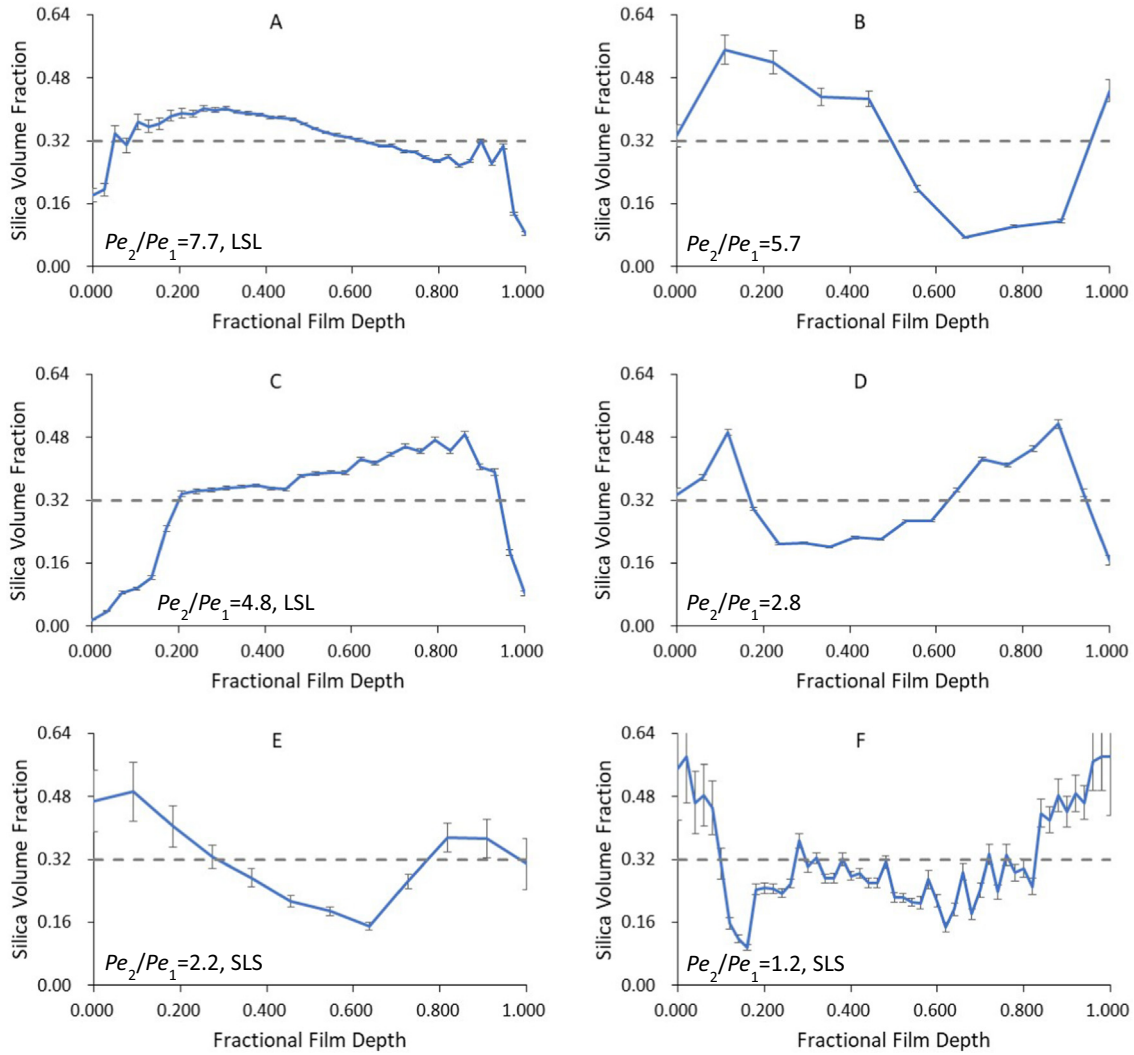

Fig. 2. Silica volume fractions at different fractional film depth of mixtures films made with (A) PS-48 and Silica-6 (Pe_2/Pe_1 = 7.7); (B) PS-48 and Silica-8 (Pe_2/Pe_1 = 5.7); (C) PS-48 and Silica-10 (Pe_2/Pe_1 = 4.8); (D) PS-48 and Silica-17 (Pe_2/Pe_1 = 2.8); (E) PS-21 and Silica-10 (Pe_2/Pe_1 = 2.2); and (F) PS-21 and Silica-17 (Pe_2/Pe_1 = 1.2). Grey dash lines represent the expected bulk volume fraction, 0.32, for silica particles in dried films.

volume fractions of silica for scaled film depths that display a more intense silica peak (Fig. 1). There are a few exceptions; the degree of stratification from data analysis for the sample with Pe_2/Pe_1 = 1.2 (Fig. 2F) is more pronounced than may be expected from looking at the peaks in these spectra, which do not show a very dramatic change throughout the film (Fig. 1F).

Relative errors in the silica volume fractions derived from the fits estimated from the coefficient of determination, R^2 were less than 5%, indicating good agreement between the data and model fit. However, the R^2 values are based on fits of a large number of data points (700–800 values of $I(q)$ at each film position); thus, the uncertainty derived from the goodness-of-fit may be an underestimate of the error. Thus, to provide a more conservative estimate of the uncertainty, the error bars shown in Fig. 2 are based on the average uncertainty in I for each film position, which we estimate based on the standard deviation of the 2D data along an arc at a particular q, err_{std}, using a 95% confidence interval (e.g. 1.96 $err_{std}/n^{1/2}$, where n is the number of data points over which err_{std} is calculated.

Our results on the type of stratification behavior are summarized in Table 2, along with the film thickness. When the size ratios are large (Fig. 2A and C, with Pe_2/Pe_1 = 7.7 and 4.8, respectively), one can see the stratification where large particles are driven upward, but also enrich the bottom, with small particles concentrated at the center. This is an interesting type of stratification behavior which has not been observed in previous studies of film stratification. We refer to this new type of stratification behavior as an "LSL" (large-small-large) structure.

Table 2
Summary of Peclet number ratios and type of stratification behavior.

Pe_2/Pe_1	Stratification behavior	Overall film thickness (μm)
7.7	LSL	400
5.7	–	100
4.8	LSL	300
2.8	–	180
2.2	SLS	120
1.2	SLS	510

Many earlier experimental and theoretical studies showed or implied only two types of stratification behavior: small-on-top or large-on-top structures. In some cases reported in previous literature, interfacial effects resulted in a small-on-top structure with a few large particles pinned to the very top surface [22,23]. However, in our experiments, each data point arises from the average scattering of a thickness of 10 μm within the sample. This is

approximately 100–1000 times of the dimension of nanoparticles. Thus, the first few data points of the top and bottom of the films represents several hundred layers of particles, and we are confident that the trends we observe are not due solely to particle interactions with the interface or the lower substrate. In Fig. 2A and C, there are at least two or more data points at both the top and bottom surfaces where the volume fraction of small particles is lower than the average throughout the film, indicated by the dashed line. Thus, the layers of large particles at the top and bottom of these films are ≥20 μm thick, and the layer of large particles at the tops of these films cannot be attributed to a few large particles, or even a monolayer of large particles, pinned at the upper surface.

Another film with a large particle size ratio but a relatively small total thickness (Pe_2/Pe_1 = 5.7, shown in Fig. 2B), is more difficult to classify. There is clearly a segregation of small and large particles in this film, but the small thickness of this sample results in a lower resolution in the SAXS experiments (i.e., fewer data points throughout the film). The data point for the topmost 10 μm of the film is very different than the data point immediately beneath it. Higher resolution of the microbeam experiments, particularly near the upper and lower surfaces of this film, are needed to classify the stratification behavior in this case.

When the size ratios are small (Pe_2/Pe_1 = 2.2 and 1.2, Fig. 2E and F, respectively), we can see the stratification with small particles enriched at the top and the bottom of films ("SLS," or small-large-small structure). The sample shown in Fig. 2D, with Pe_2/Pe_1 = 2.8, also seems to show SLS behavior, although as in Fig. 2B, the data point corresponding to the topmost 10 μm of the film is

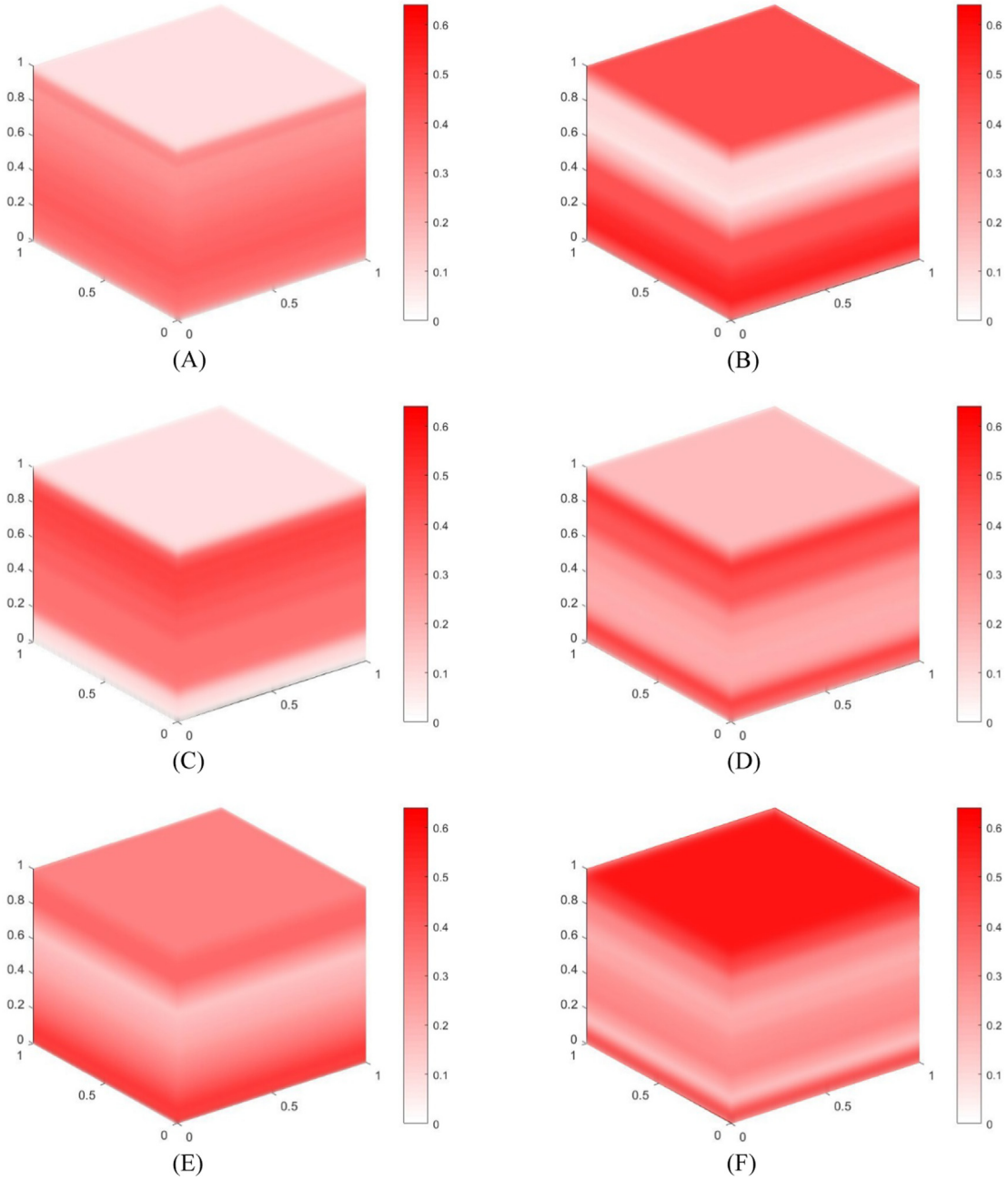

Fig. 3. Illustrations of film structures with nanoparticle size ratios: (A) 7.7; (B) 5.7; (C) 4.8; (D) 2.8; (E) 2.16; and (F) 1.2. Color bars indicate corresponding silica volume fraction, 0–0.64, (Darker red indicates higher silica volume fraction, and lighter red/white indicated lower silica volume fraction). Interpolation between data points was made to simulate smooth concentration change. (For interpretation of the references to colour in this figure legend, the reader is referred to the web version of this article.)

very different than the layer immediately beneath it, and higher resolution of the composition in the vertical direction would be desirable.

Among the "LSL" films, the film with the largest size ratio, 7.7, appears to have the smallest degree of stratification. Although this does not agree with our expectations from diffusive theories of stratification, it is consistent with trends seen in our earlier AFM studies. The difference in the degree of stratification is small among "SLS" films. This may be because the differences in size ratio are not as large.

In order to visualize how particles arranged and compare the difference in the extent of stratification among films, illustrations generated from results are made using MATLAB. GIMP software was used to blur the color change between layers to mimic smooth composition changes, which is essentially an interpolation (Fig. 3A–F).

3.3. Possible mechanism of LSL and SLS layering

As discussed above, many earlier experimental and theoretical studies showed only small-on-top or large-on-top structures, other than a few simulation studies that found small-on-top stratification with a few large particles pinned to the upper surface [22,23]. Thus, a natural question is what type of physics or mechanism could lead to such a structure. One major difference between many modeling studies and our experimental study is the presence of interparticle interactions. Several early modeling studies of stratification assume that the particles differ only in size [15]. However, our zeta potential measurements suggest that there is likely an interparticle attraction between the PS and silica particles in our system. Very strong PS-silica attractions could result in formation of large aggregates, but we do not see evidence of aggregation in our scattering spectra. However, weak PS-silica attractions could modify the expected stratification behavior, as shown by the modeling work of Zhou et al. [24], who show that cross-interactions can lead to different types of stratification behavior depending upon both the particle *Pe* and the initial volume fraction of small particles. Our experiments are at a lower initial volume fraction of silica than previous experimental studies by our group [31], supporting the idea that the initial volume fraction of particles is likely an important parameter in obtaining different types of stratification behavior. However, even the modeling work of Zhou et al. [24] does not show a regime with LSL or SLS layering. We expect that another factor that may lead to sandwich-type layering is jamming of particle layers late in the drying process; to our knowledge, this has not been accounted for in the models of stratification that have been presented to date. The state diagrams derived by Zhou et al. [24] are based on modeling that has been performed until the films are half of their initial height, and are hence only partially dried. If, for example, a layer enriched in large particles forms at the top of the film later in the drying process and becomes jammed, this layer would persist even if other effects are driving small particles upward.

4. Conclusions

We have successfully utilized SAXS experiments with an X-ray microbeam as a novel method to study the depth-resolved structures of binary mixture films. SAXS patterns with small variations at different depths of films were captured and fit to get quantitative results on particle compositions. Based on previous theoretical work [15,19,21–24,26,27], we hypothesized that varying the ratio of particle Peclet numbers would lead to either small-on-top stratification, large-on-top stratification, or uniform films. However, we observed two new types of stratification behavior, large-small-large or "LSL" film structures, which we tend to find at large nanoparticle size ratios; and small-large-small or "SLS" film structures, which is observed at small size ratios. To our knowledge, these interesting "sandwich" structures in binary colloidal films have not been predicted by previous theories or observed in earlier experimental studies. Francis and co-workers have seen experimental evidence of sandwich layering during the drying process in single-component films [30], although because these are single-component films, the structure does not persist for the final dried film; while Routh and co-workers have experimentally observed large-on-top stratification [16] and Keddie and colleagues have observed mainly small-on-top stratification in experiments [29]. It is important to note that we have kept the initial volume fraction of both particles fixed in these studies. Other types of stratification behavior (small-on-top, large-on-top) may be favored for small and large particle size ratios as the initial volume fraction is varied, so our results are not necessarily in conflict with earlier studies that show other structures. However, these experiments provide some insight that can be used to drive future theoretical and experimental developments in film drying, colloidal stratification, and evaporative assembly. We expect that cross-particle interactions, as well as jamming during late stages of the drying process, may be important in designing processes that produce more complex layered structures. Additionally, development of other experimental approaches to study stratification, such as confocal microscopy, may be useful, although challenges remain in quantifying the particle volume fraction obtained from such measurements. Collectively, these can guide design of improved single-step processes for production of multicomponent nanoparticle films.

Acknowledgement

Financial support for this work was provided by the National Science Foundation through award CBET-1335787 and a Department of Education Graduate Assistance in Areas of National Need (GAANN) fellowship for A.J.C., Award P200A160163. This research used resources of the Center for Functional Nanomaterials, and the National Synchrotron Light Source II, U.S. Department of Energy (DOE) Office of Science User Facilities operated for the DOE Office of Science by Brookhaven National Laboratory under Contract No. DE-SC0012704.

Appendix A. Supplementary material

Supplementary data to this article can be found online at https://doi.org/10.1016/j.jcis.2018.11.084.

References

[1] H. Philamore, J. Rossiter, P. Walters, J. Winfield, I. Ieropoulos, Cast and 3D printed ion exchange membranes for monolithic microbial fuel cell fabrication, J. Power Sources 289 (2015) 91–99.
[2] B. Dunn, J.W. Long, D.R. Ronson, Rethinking multifunction in three dimensions for miniaturizing electrical energy storage, Electrochem. Soc. Interface 17 (3) (2008) 49.
[3] G. Gebresilassie Eshetu, M. Armand, B. Scrosati, S. Passerini, Energy storage materials synthesized from ionic liquids, Angew. Chem. Int. Ed. 53 (49) (2014) 13342–13359.
[4] K.C. Krogman, T. Druffel, M.K. Sunkara, Anti-reflective optical coatings incorporating nanoparticles, Nanotechnology 16 (7) (2005) S338.
[5] C.H. Hsu, Electrically conducting organic polymer/nanoparticle composites and method for use there of U.S. Patent 8 (2013) 455–865.
[6] M. Irimia-Vladu, "Green" electronics: biodegradable and biocompatible materials and devices for sustainable future, Chem. Soc. Rev. 43 (2) (2014) 588–610.
[7] T.W. Oppel, W.K. Myers, C.S. Keefer, The sedimentation rate of the red blood cells in various types of arthritis, J. Clin. Invest. 12 (2) (1933) 291.
[8] I. Nikiforow, J.r. Adams, A.M. König, A. Langhoff, K. Pohl, A. Turshatov, D. Johannsmann, Self-stratification during film formation from latex blends

driven by differences in collective diffusivity, Langmuir 26 (16) (2010) 13162–13167.
[9] J. Keddie, A.F. Routh, Fundamentals of Latex Film Formation: Processes and Properties, Springer Science Media, 2010.
[10] J.L. Keddie, Film formation of latex, Mater. Sci. Eng.: R: Rep. 21 (3) (1997) 101–170.
[11] S. Kiil, Drying of latex films and coatings: reconsidering the fundamental mechanisms, Prog. Org. Coat. 57 (3) (2006) 236–250.
[12] A.F. Routh, W.B. Russel, Horizontal drying fronts during solvent evaporation from latex films, AIChE J. 44 (9) (1998) 2088–2098.
[13] A.F. Routh, W.B. Russel, A process model for latex film formation: limiting regimes for individual driving forces, Langmuir 15 (22) (1999) 7762–7773.
[14] A.F. Routh, W.B. Russel, Deformation mechanisms during latex film formation: experimental evidence, Ind. Eng. Chem. Res. 40 (20) (2001) 4302–4308.
[15] R. Trueman, E.L. Domingues, S. Emmett, M. Murray, A. Routh, Auto-stratification in drying colloidal dispersions: a diffusive model, J. Colloid Interface Sci. 377 (1) (2012) 207–212.
[16] R. Trueman, E. Lago Domingues, S. Emmett, M. Murray, J. Keddie, A. Routh, Autostratification in drying colloidal dispersions: experimental investigations, Langmuir 28 (7) (2012) 3420–3428.
[17] A.K. Atmuri, S.R. Bhatia, A.F. Routh, Autostratification in drying colloidal dispersions: effect of particle interactions, Langmuir 28 (5) (2012) 2652–2658.
[18] S. Cheng, G.S. Grest, Dispersing nanoparticles in a polymer film via solvent evaporation, ACS Macro Lett. 5 (6) (2016) 694–698.
[19] A. Fortini, I. Martín-Fabiani, J.L. De La Haye, P.-Y. Dugas, M. Lansalot, F. D'Agosto, E. Bourgeat-Lami, J.L. Keddie, R.P. Sear, Dynamic stratification in drying films of colloidal mixtures, Phys. Rev. Lett. 116 (11) (2016) 118301.
[20] H. Luo, C.M. Cardinal, L. Scriven, L.F. Francis, Ceramic nanoparticle/monodisperse latex coatings, Langmuir 24 (10) (2008) 5552–5561.
[21] A. Fortini, R.P. Sear, Stratification and size segregation of ternary and polydisperse colloidal suspensions during drying, Langmuir 33 (19) (2017) 4796–4805.
[22] M.P. Howard, A. Nikoubashman, A.Z. Panagiotopoulos, Stratification dynamics in drying colloidal mixtures, Langmuir 33 (15) (2017) 3685–3693.
[23] M.P. Howard, A. Nikoubashman, A.Z. Panagiotopoulos, Stratification in drying polymer-polymer and colloid-polymer mixtures, Langmuir 33 (42) (2017) 11390–11398.
[24] J. Zhou, Y. Jiang, M. Doi, Cross interaction drives stratification in drying film of binary colloidal mixtures, Phys. Rev. Lett. 118 (10) (2017) 108002.
[25] R.P. Sear, P.B. Warren, Diffusiophoresis in non-adsorbing polymer solutions: the Asakura-Oosawa model and stratification in drying films, Phys. Rev. E 96 (6) (2017) 062602.
[26] R.P. Sear, Stratification of mixtures in evaporating liquid films occurs only for a range of volume fractions of the smaller component, J. Chem. Phys. 148 (13) (2018) 134909.
[27] Y. Tang, G.S. Grest, S. Cheng, Stratification in drying films containing bidisperse mixtures of nanoparticles, Langmuir 34 (24) (2018) 7161–7170.
[28] X. Liu, W. Liu, A.J. Carr, D.S. Vazquez, D. Nykypanchuk, P.W. Majewski, A.F. Routh, S.R. Bhatia, Stratification during evaporative assembly of multicomponent nanoparticle films, J. Colloid Interface Sci. 515 (2018) 70–77.
[29] D. Makepeace, A. Fortini, A. Markov, P. Locatelli, C. Lindsay, S. Moorhouse, R. Lind, R. Sear, J. Keddie, Stratification in binary colloidal polymer films: experiment and simulations, Soft Matter 13 (39) (2017) 6969–6980.
[30] C.M. Cardinal, Y.D. Jung, K.H. Ahn, L. Francis, Drying regime maps for particulate coatings, AIChE J. 56 (11) (2010) 2769–2780.
[31] A.J. Carr, W. Liu, K.G. Yager, A.F. Routh, S.R. Bhatia, Evidence of stratification in binary colloidal films from microbeam X-ray scattering: toward optimizing the evaporative assembly processes for coatings, ACS Appl. Nano Mater. 1 (8) (2018) 4211–4217.
[32] N. Dingenouts, M. Ballauff, Assessment of spatial order in dried latexes by small-angle X-ray scattering, Macromolecules 31 (21) (1998) 7423–7429.
[33] N. Dingenouts, M. Ballauff, First stage of film formation by latexes investigated by small-angle X-ray scattering, Langmuir 15 (9) (1999) 3283–3288.
[34] J. Li, B. Cabane, M. Sztucki, J. Gummel, L. Goehring, Drying dip-coated colloidal films, Langmuir 28 (1) (2011) 200–208.
[35] W.M. Haynes, CRC Handbook of Chemistry and Physics, CRC Press, 2014.
[36] J.E. Mark, Polymer Data Handbook, Oxford University Press (2009).